Axial Ligand Field in D4d Coordination Symmetry: Magnetic Relaxation of Dy SMMs Perturbed by Counteranions

Jianfeng Wu, Olivier Cador, Xiao-Lei Li, Lang Zhao, Boris Le Guennic, Jinkui Tang

Axial Ligand Field in D_{4d} Coordination Symmetry: Magnetic Relaxation of Dy SMMs Perturbed by Counter-anions

Jianfeng Wu,[†] Olivier Cador,[‡] Xiao-Lei Li,[†] Lang Zhao,[†] Boris Le Guennic*,[‡] and Jinkui Tang*,[†]

[†]State Key Laboratory of Rare Earth Resource Utilization, Changchun Institute of Applied Chemistry, Chinese Academy of Sciences, Changchun 130022, P. R. China

[‡]Institut des Sciences Chimiques de Rennes, UMR 6226 CNRS-Université de Rennes 1, 263 Avenue du General Leclerc, 35042 Rennes Cedex, France

ABSTRACT: A series of mononuclear Dy^{III} complexes with the general formula $[DyLz_2(salicylaldehyde)_2]\cdot X\cdot solvent$ (Lz = 6-Pyridin-2-yl-[1,3,5]triazine-2,4-diamine; X = OH^- (**1·OH**), Cl^- (**2·Cl**), Br^- (**3·Br**)) have been synthesized using mixed salicylaldehyde/pyridin-triazine ligands and discriminative counter-anions. The Dy^{III} ion in these three complexes resides in a similar D_{4d} coordination geometry with counter-anions perturbing the coordination environment and bond lengths and angles in the lattice. Magneto-structural studies reveal that the asymmetric distribution of salicylaldehyde/pyridin-triazine ligands and the presence of discriminative counter-anion result in the coexistence of large anisotropy and quantum tunneling of magnetization. The magnetic anisotropy is dominated by the axial ligand field with short Dy-O_{sali} distances and large $\angle O_{sali}$-Dy-O_{sali} angles, while the quantum tunneling relaxation is probably dictated by the π-π stacking of the Lz ligands which induces an axial constriction of the coordinating plane. *Ab initio* calculations substantiate the diversity of the magnetic behaviors in these complexes and highlight the importance of axial ligand field with short Dy-O_{sali} distances, large $\angle O_{sali}$-Dy-O_{sali} angles and less ligand stacking in these pseudo-D_{4d} symmetrical single-molecule magnets.

INTRODUCTION

Since the discovery of single-molecule magnetic behavior in the celebrated molecule of $(Bu_4N)[Tb(Pc)_2]$ (H_2Pc = phthalocyanine) in 2003,[1] the research on lanthanide single-molecule magnets (SMMs) has been well developed and hundreds of lanthanide compounds with diverse structural topologies have been reported in the past decade.[2-8] Compared with transition elements, lanthanide ions provide larger magnetic moments and more significant magnetic anisotropy profiting from the strong coupling between the spin and orbit angular moments and the weak crystal-field splitting effects,[9-12] thus making them ideal candidates for the construction of SMMs. However the relatively weak magnetic coupling between lanthanide ions in multinuclear compounds limits the performance of robust SMM behavior, except for low-symmetry dysprosium compounds, such as Dy_5,[13] Dy_4K_2,[14] Dy_3[15] and Dy_2[16-19] complexes. According to the crystal field approach toward 4f SMMs,[20-22] the splitting of the $^{2S+1}L_J$ multiplets varies with the coordination symmetry of the lanthanide ion and determines the magnetic anisotropy and magnetic relaxation behavior.[23-28] Theoretically speaking, lanthanide SMMs with high symmetry, such as C_3, S_8, D_{4d}, D_{5h} and D_{6d}, are inclined to show very high-energy barriers and less quantum tunneling of magnetization (QTM).[29-33] Indeed, a series of Dy^{III}, Tb^{III} and Er^{III} based mononuclear SMMs with landmark significance have been reported showing the above symmetries and robust anisotropy barriers and blocking temperatures.[1, 34-36]

On the other hand, a simple but amenable electrostatic model based on basic overall shape of free-ion electron density has been widely used recently to understand and predict the magnetic anisotropy of lanthanide SMMs.[37-39] For instance, the Kramers ion Er^{III} ($^4I_{15/2}$) and Dy^{III} ($^6H_{15/2}$) with prolate and oblate shaped electron density would provide large magnetic anisotropy in highly equatorial and strongly axial ligand field, respectively.[40-44] In particular, the later oblate shaped Dy^{III} ion in near-perfect pentagonal bipyramidal symmetry with weak equatorial pyridine donors and strong *tert*-butoxide donors was reported recently showing record energy barrier of 1815 K.[34] The anionic character of coordinate donors and the steric tunability of counter-anion may be exploited to stabilize the 4f electronic density.[37, 45, 46] Therefore, rational optimization of the ligand field around a lanthanide ion is the key step to obtain high performance SMMs.[22, 47]

On the basis of above theoretical and conceptual aspects, we intend to design SMMs based on Dy^{III} ion with

high coordination number and strong axial ligand field, such as eight coordinate Dy^{III} in D_{4d} symmetry, which are stable in both solid-state and frozen solution.[48-56] Recently, we obtained a series of mononuclear dysprosium complexes with a Dy^{III} ion located in approximate D_{4d} coordination geometry and two *o*-vanilin in *trans* configuration (Scheme 1), showing remarkable relaxation barrier and blocking temperature.[57] In the present work, we replaced the *o*-vanilin with salicylaldehyde and used halogen as counter anions, and obtained a series of mononuclear dysprosium complexes of formula $[DyLz_2(salicylaldehyde)_2]\cdot X\cdot solvent$ (Lz = 6-Pyridin-2-yl-[1,3,5]triazine-2,4-diamine; X = OH^- (**1·OH**), Cl^- (**2·Cl**), Br^- (**3·Br**)). In these complexes, the magnetic relaxation barrier varies largely according to the change of counter anions. Magneto-structural studies and *ab initio* calculations indicate that the magnetic anisotropy is dominated by the short Dy-O_{sali} distances and large $\angle O_{sali}$-Dy-O_{sali} angles in the pseudo-D_{4d} geometry.

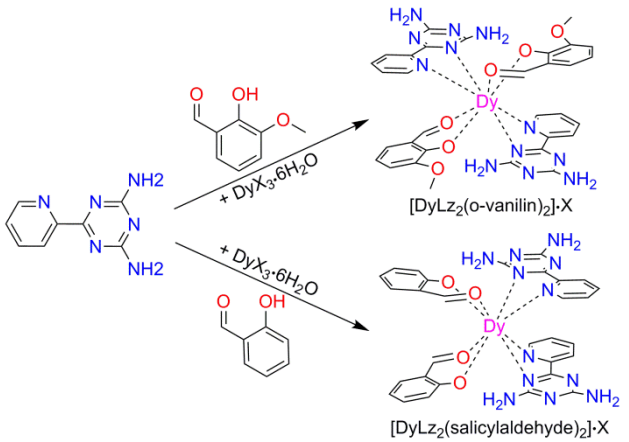

Scheme 1 Preparation of the complexes $[DyLz_2(o\text{-vanilin})_2]\cdot X$ and $[DyLz_2(salicylaldehyde)_2]\cdot X$.

EXPERIMENTAL

General Synthetic Considerations. All chemicals and solvents were commercially obtained and used as received without any further purification. FTIR spectra were measured using a Nicolet 6700 Flex FTIR spectrometer equipped with smart iTR™ attenuated total reflectance (ATR) sampling accessory in the range from 500 to 4000 cm^{-1}. Elemental analysis for C, H and N were carried out on a Perkin-Elmer 2400 analyzer. Ligand Lz (2,4-diamino-6-pyridyl-l,3,5-triazines) was prepared according to a previously published method under ambient conditions.[58] All doped samples were analyzed using Inductively Coupled Plasma Optical Emission Spectrometry (ICP OES). Powder X-ray diffraction measurements were recorded on Bruker D8 advance X-Ray diffractometer using Cu-Kα radiation.

Synthesis of 1·OH. $Dy(SO_3CF_3)_3\cdot 6H_2O$ (0.2 mmol) was added to a solution of Lz (0.2 mmol) and salicylaldehyde (0.2 mmol) in 15 mL mixture of methanol and dichloromethane (1:2, v/v), and then triethylamine (0.4 mmol) was added. The resultant solution was stirred for 3 h and subsequently filtered. The filtrate was exposed to air to allow the slow evaporation of the solvent. Yellow crystals of **1·OH** suitable for X-ray diffraction analysis were collected after 1 week. Yield in ~ 70%. Selected IR (cm^{-1}) for **1·OH**: 3336 (m), 3145 (b), 1619 (s), 1535 (s), 1440 (m), 1397 (w), 1322 (s), 1244 (s) 1147 (s), 1025 (m), 900 (s), 792 (m), 760 (m), 637 (m). Anal. Calcd. for $[DyLz_2(salicylaldehyde)_2]\cdot OH\cdot 2CH_3OH$ ($C_{32}H_{35}DyN_{12}O_7$, MW = 862.22): C, 44.58%; H, 4.09%; N, 19.49%. Found: C, 44.36%; H, 3.98%; N, 19.58%. Doping of complex **1·OH** was performed by adding $Dy(SO_3CF_3)_3\cdot 6H_2O$ and $Y(SO_3CF_3)_3\cdot 6H_2O$ together (with the ratio of 1:20) in the synthesis process. ICP OES analysis found $[Dy_{0.067}Y_{0.933}Lz_2(salicylaldehyde)_2]\cdot OH\cdot 2CH_3OH$.

Syntheses of complexes 2·Cl and 3·Br. Complexes **2·Cl** and **3·Br** were synthesized using a similar procedure as for **1·OH** with the replacement of $Dy(SO_3CF_3)_3\cdot 6H_2O$ by $DyCl_3\cdot 6H_2O$ and $DyBr_3\cdot 6H_2O$, respectively. Selected IR (cm^{-1}) for **2·Cl**: 3273 (m), 3130 (b), 1617 (s), 1580 (w), 1561 (w), 1536 (s), 1510 (m), 1437 (m), 1392 (m), 1325 (s), 1257 (w), 1184 (m) 1147 (s), 1014 (m), 900 (s), 791 (m), 769 (m), 625 (m), 589 (w). Anal. Calcd. for $[DyLz_2(salicylaldehyde)_2]\cdot Cl\cdot H_2O$ ($C_{31}H_{30}ClDyN_{12}O_5$, MW = 848.62): C, 43.88%; H, 3.56%; N, 19.81%. Found: C, 43.81%; H, 3.68%; N, 20.04%. Selected IR (cm^{-1}) for **3·Br**: 3296 (m), 3133 (b), 1618 (s), 1535 (s), 1512 (m), 1437 (m), 1392 (m), 1325 (s), 1196 (m) 1149 (s), 1014 (m), 900 (s), 791 (m), 767 (m), 589 (m). Anal. Calcd. for $[DyLz_2(salicylaldehyde)_2]\cdot Br\cdot H_2O\cdot CH_3OH$ ($C_{31}H_{32}BrDyN_{12}O_6$, MW = 911.10): C, 40.87%; H, 3.54%; N, 18.45%. Found: C, 40.72%; H, 3.68%; N, 18.57%. Doping of complex **2·Cl** was performed by adding $DyCl_3\cdot 6H_2O$ and $YCl_3\cdot 6H_2O$ together (with the ratio of 1:20) in the synthesis process. ICP OES analysis found $[Dy_{0.058}Y_{0.942}Lz_2(salicylaldehyde)_2]\cdot Cl\cdot H_2O$.

Crystallography. Single-crystal X-ray data of the titled complexes were collected on a Bruker Apex II CCD diffractometer equipped with graphite-monochromatized Mo-Kα radiation (λ = 0.71073 Å) at 293(2) K. The structures were solved by direct methods and refined by full-matrix least-squares methods on F^2 using SHELXTL-2014.[59, 60] All non-hydrogen atoms in the whole structure were refined with anisotropic displacement parameters. Hydrogen atoms were introduced in calculated positions and refined with fixed geometry with respect to their carrier atoms. Crystallographic data are listed in Table S1. CCDC 1513743-1513745 contain the supplementary crystallographic data for this paper. These data can be obtained free of charge from the Cambridge Crystallographic Data Centre via www.ccdc.cam.ac.uk/data_request/cif.

Magnetic Measurements. Magnetic susceptibility measurements were recorded on a Quantum Design

MPMS-XL7 SQUID magnetometer equipped with a 7 T magnet. Direct current (dc) magnetic susceptibility measurements were performed on a polycrystalline samples of **1·OH**, **2·Cl** and **3·Br** in the temperature range 2–300 K, in an applied field of 1000 Oe. The variable-temperature magnetization was measured in the temperature range of 1.9–300 K. The dynamics of the magnetization were investigated from the ac susceptibility measurements in the zero static fields and a 3.0 Oe ac oscillating field. Diamagnetic corrections were made with the Pascal's constants[61] for all the constituent atoms as well as the contributions of the sample holder.

Table 1. Selected bond distances (Å) and angles (°) for complexes **1·OH**, **2·Cl** and **3·Br**.

	1·OH		2·Cl	3·Br
Dy1-O1	2.365(5)	Dy1-O1	2.252(6)	2.237(7)
Dy1-O1' [a)]	2.365(5)	Dy1-O2	2.356(7)	2.352(7)
Dy1-O2	2.203(5)	Dy1-O3	2.242(6)	2.241(7)
Dy1-O2'	2.203(5)	Dy1-O4	2.369(6)	2.366(7)
Dy1-N1	2.509(6)	Dy1-N1	2.513(8)	2.503(8)
Dy1-N1'	2.509(6)	Dy1-N6	2.593(7)	2.572(7)
Dy1-N6	2.593(5)	Dy1-N7	2.519(7)	2.522(8)
Dy1-N6'	2.593(5)	Dy1-N12	2.591(7)	2.588(7)
O2-Dy1-O2'	149.018	O1-Dy1-O3	142.855	142.958
Dy···Dy	7.682	Dy···Dy	8.093	8.080
$\pi\cdots\pi$ / Å [b)]	3.826	$\pi\cdots\pi$ / Å	3.596	3.590
ϕ / ° [c)]	58.646	ϕ / °	46.946	46.942
θ / ° [d)]	6.841	θ / °	2.525	2.593
d_{pp} / Å [e)]	2.639	d_{pp} / Å	2.613	2.619

[a)] Symmetry transformation: 1 -x, -y+3/2, z. [b)] Distance between the centers of the triazine groups. [c)] Angle defined as the rotation angle between the two Lz ligands. [d)] Angle between the upper and lower planes containing the coordinated atoms. [e)] The sum distance from the center Dy^{III} ion to two coordination planes.

***Ab initio* Calculations.** Wavefunction-based calculations were carried out on the X-ray structures of **1·OH**, **2·Cl** and **3·Br** using the SA-CASSCF/RASSI-SO approach as implemented in MOLCAS 8.0,[62] in which the relativistic effects are treated by means of the Douglas-Kroll Hamiltonian in a two steps scheme. First, the scalar terms are included in the basis-set generation and are used to determine the spin-free states in the Complete Active Space Self-Consistent Field (CASSCF) method.[63] Next, spin-orbit coupling is added within the Restricted Active Space State-Interaction (RASSI-SO) method,[64, 65] in which the spin-free states serve as basis states. The resulting energies and wave functions are finally used to compute the magnetic properties (*i.e.* magnetization and magnetic susceptibility curves, anisotropy tensors of the low-energy states of the system, as well as the associated wave functions in term of M_J eigenstates) using the pseudo-spin S = 1/2 approximation as defined in the SINGLE_ANISO routine.[66, 67] Cholesky decomposition is used when computing bielectronic integrals.[68] The active space of the CASSCF calculations consisted of the nine 4f electrons of the Dy^{III} ion spanning the seven 4f orbitals, *i.e.* CAS(9,7)SCF. The State-Averaged CASSCF calculations were performed for all the 21 sextet roots, all the 224 quadruplet roots and 300 out of 490 doublet roots. In the RASSI-SO calculation, the 21 sextet roots were allowed to mix through spin-orbit coupling with the first 128 quadruplet roots and the first 107 doublet roots. All atoms were described by ANO-type basis sets from the ANO-RCC library of MOLCAS.[69-71] The following contractions were used: [8s7p4d3f2g1h] for the Dy^{III} ion, [4s3p2d] for the four N and the four O atoms of the first coordination sphere, [3s2p1d] for the remaining N atoms and all C atoms, and [2s] for the H atoms.

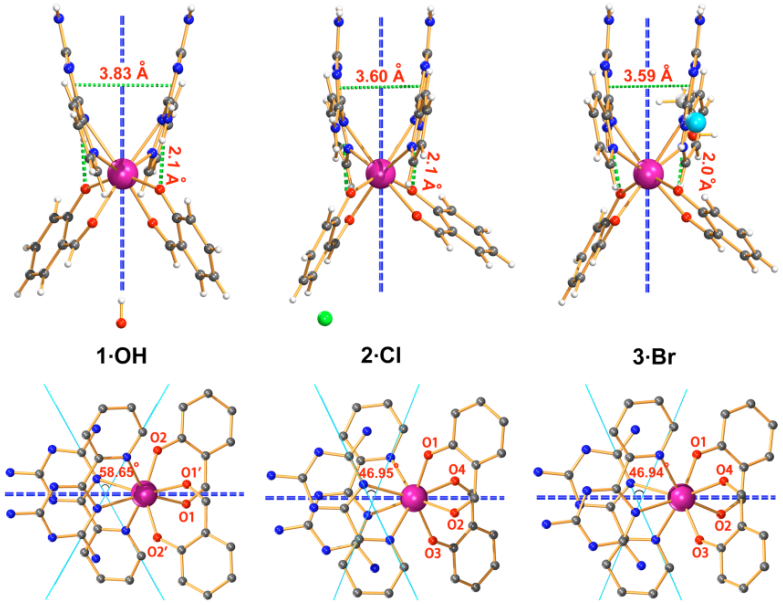

Figure 1. Side (top) and top (bottom) views of complexes **1·OH**, **2·Cl** and **3·Br** with parameter labels. The dashed blue lines represent the location of the pseudo-C_2 molecular axes. The crossed solid azure lines represent the orientations of the two Lz ligands with labeled rotation angle (ϕ). The pink, blue, dark grey, red, green and azure spheres represent Dy, N, C, O, Cl and Br atoms, respectively; solvents (top) and/or hydrogen atoms (bottom) have been omitted for clarity.

RESULTS AND DISCUSSION

Structural Descriptions. Compounds **1·OH**, **2·Cl** and **3·Br** were isolated from the reaction of $DyX_3{\cdot}6H_2O$ (X = $CF_3SO_3^-$ for **1·OH**, Cl^- for **2·Cl**, Br^- for **3·Br**) with Lz and salicylaldehyde in the presence of triethylamine in 15 mL mixture of methanol and dichloromethane (1:2, v/v) after several days (Scheme 1). Details for the structure solution and refinement are summarized in Table S1. Powder XRD analyses are given in Figure S2. Selected bond distances and angles are given in Table 1. Single-crystal X-ray diffraction analyses (Figure 1, Table S1) show that complex **1·OH** crystallizes in the tetragonal *I41/a* space group with the asymmetric unit containing half of the complex (one ligand Lz and one ligand salicylaldehyde and one half Dy^{III} ion). Complexes **2·Cl** and **3·Br** crystallize in the triclinic *P-1* space group with the asymmetric unit containing two ligands Lz, two salicylaldehyde and one Dy^{III} ion. The metallic core arrangements of **1·OH**, **2·Cl** and **3·Br** are identical, each displaying a sandwich-like structure in which the ligands Lz and salicylaldehyde construct two coordinate planes with the Dy^{III} ion sandwiched between them. The Dy^{III} ion is eight coordinated and resides in a square-antiprismatic environment where the planes are constructed by hydrogen bonding-associated Lz and salicylaldehyde ligands through the hydroxy oxygen of the salicylaldehyde and one hydrogen atom of the Lz ligand (Figure 1). Each complex is further charge balanced by counter ions in the lattice. Thus the only chemical differences found between the three complexes are the counter ions (OH^- for **1·OH**, Cl^- for **2·Cl** and Br^- for **3·Br**). Because of the different counter ions in **1·OH**, **2·Cl** and **3·Br**, the complexes display distinct properties that distinguish each other.

Structural Comparisons. As shown in Figure 1 and Table 1, the variation of counter ion in the lattice results in the modification of the coordination environment as well as the arrangement of ligands. In all three complexes, the Lz and salicylaldehyde ligands are in *cis* configuration relative to each other with the average Dy-N distance of 2.55 Å (for all three complexes) and Dy-O distances of 2.28 (**1·OH**) and 2.30 Å (**2·Cl** and **3·Br**). The anionic donor O atoms are far closer to the Dy^{III} ion than the neutral N atoms, highlighted by the Dy-O_{sali} distances, $\angle O_{sali}$-Dy-O_{sali} angles (here the O_{sali} represents the hydroxy oxygen of the salicylaldehyde) and π···π stacking effects of ligands Lz, creating a predominantly axial distribution of the electronic structure. A closer look at the structure reveals that the Dy-O_{sali} distances and $\angle O_{sali}$-Dy-O_{sali} angles are dominated by the distance and angle between the upper and lower coordinate planes (θ) as well as the rotation angle between them (ϕ). In complex **1·OH**, a relatively large θ angle (6.84°) with respect to **2·Cl** (2.53°) and **3·Br** (2.59°) indicates a constriction of the coordinate planes at the O_{sali} atoms side (Figure S1), resulting in a short Dy-O_{sali} distance of 2.20 Å (2.25 and 2.24 Å for **2·Cl**, 2.24 Å for **3·Br**, Tables 1 and S3). The $\angle O_{sali}$-Dy-O_{sali} angle of 149.02° for **1·OH** is larger than 142.86° for **2·Cl** and 142.96° for **3·Br** (140.46° for perfect D_{4d} geometry), which is also consistent with the large ϕ angle of 58.65° for **1·OH** (46.95°, 46.94° for **2·Cl** and **3·Br**, respectively). The π···π stacking effects are also influenced by the rotation angles ϕ of the Lz ligands. When the ϕ angles increase, the π···π distances get larger, therefore the π···π distance of 3.826 Å for **1·OH** is larger than the values of 3.596 Å, 3.590 Å for **2·Cl** and **3·Br** (Table 1). The SHAPE software[72] was used to quantify the coordination geometry of the Dy^{III} center and gave the continuous shape measure deviations (CSMD) of 1.327, 0.643 and 0.725 for **1·OH**, **2·Cl** and **3·Br** (Table S2, D_{4d} coordination symetry), respectively. This demonstrates that the coordination polyhedron in **1·OH** is more distorted than in **2·Cl** and **3·Br**. Moreover, we investigated the closest intermolecular Dy···Dy distances to check their effects on the dynamical magnetic properties. In the case of complex **1·OH**, the relatively short Dy···Dy distance (7.68 Å) does not necessarily preclude weak dipolar interactions since the later are also governed by the angles between the magnetic moments (*vide infra*). The Dy···Dy distances in **2·Cl** (8.09 Å) and in **3·Br** (8.08 Å) are a little longer, which also suggests the presence of potential weak intermolecular magnetic interactions.

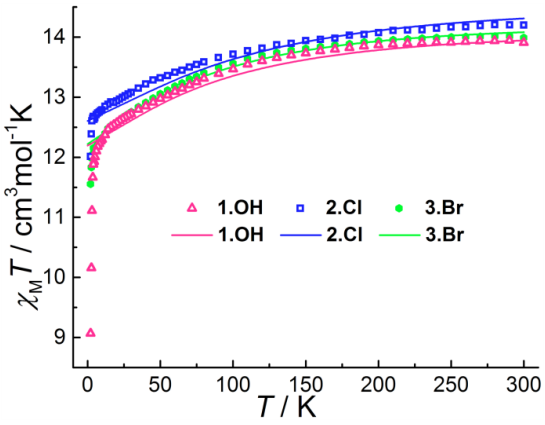

Figure 2. Temperature dependence of $\chi_M T$ product at 1 kOe for **1·OH** (red), **2·Cl** (blue) and **3·Br** (green). The solid lines correspond to *ab initio* calculations.

Magnetic properties. In order to probe the magnetic properties, direct current (dc) magnetic susceptibility measurements were collected on polycrystalline samples under an applied field of 1 kOe in the temperature range 2–300 K. The $\chi_M T$ (χ_M molar magnetic susceptibility) *vs.* T plots for **1·OH**, **2·Cl** and **3·Br** (Figure 2), reveal the room temperature $\chi_M T$ values of 13.91, 14.18 and 13.91 $cm^3 \cdot K \cdot mol^{-1}$, respectively, which are in good agreement with the value expected for the free-ion approximation of Dy^{III} ions (S = 5/2, L = 5, $^6H_{15/2}$, g = 4/3, C = 14.17 $cm^3 \cdot K \cdot mol^{-1}$). When reducing the temperature, the $\chi_M T$ value gradually decreases before a sharp drop below 15 K, reaching the values of 9.07, 12.01 and 11.56 $cm^3 \cdot K \cdot mol^{-1}$ for **1·OH**, **2·Cl** and **3·Br**, respectively. The high temperature decrease can be attributed to the depopulation of the

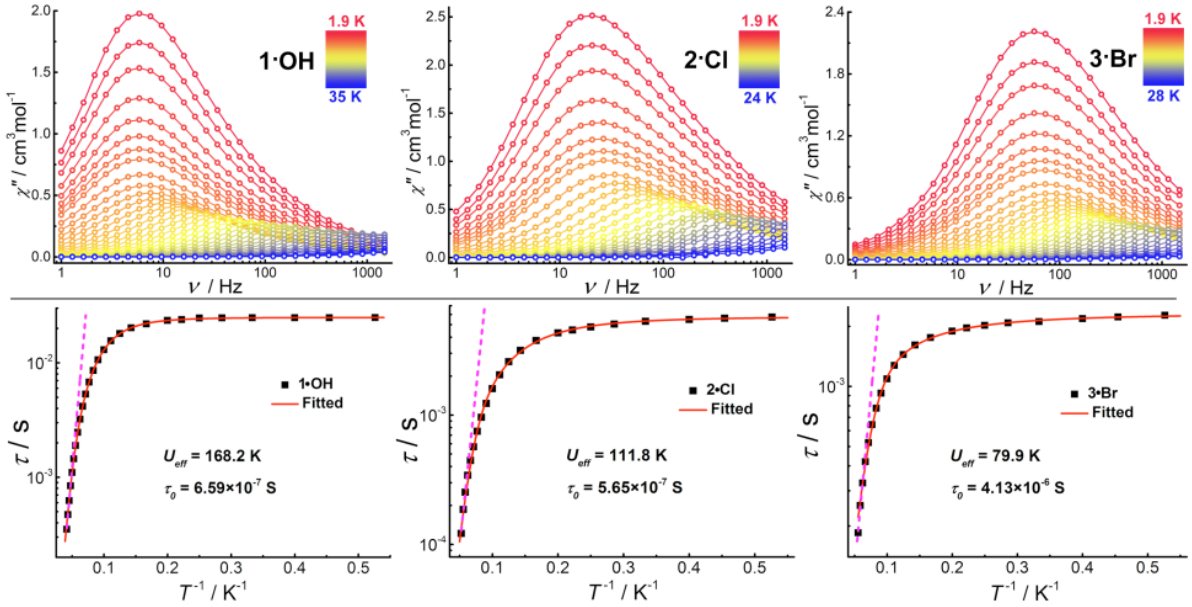

Figure 3. Frequency-dependent out of phase ac susceptibilities (top) and plots of τ *vs.* T^{-1} (bottom) for **1·OH** (left), **2·Cl** (middle) and **3·Br** (right) under zero dc field. The red line represents the fitting to eq. 1, pink dash line represents the Arrhenius fitted result.

excited m_J sublevels of the ground J states of the Dy^{III} ions, while the sharp drop at lower temperature region suggests non-negligible dipolar interactions between the neighboring Dy^{III} ions, especially for **1·OH** (shortest Dy···Dy distance of 7.68 Å). The isothermal molar magnetization (M) *vs.* H plots for **1·OH**, **2·Cl** and **3·Br** (Figures S3-S5) show sharp increase with increasing H at low fields and then linear increases at high fields, reaching the values of 5.32, 5.31 and 5.48 μ_B at 5 T, for **1·OH**, **2·Cl** and **3·Br**, respectively, which are very close to the expected value of 5 μ_B for Dy^{III} ions in a pure $m_J = |\pm 15/2>$ ground state.

Variable temperature and frequency alternating current (ac) susceptibility measurements were also performed to probe the slow relaxation of the magnetization and quantum tunneling effects within these molecules, utilizing a 3 Oe oscillating field and a zero-applied direct current. Both the in-phase (χ') and out-of-phase (χ'') susceptibilities display a temperature (Figure S6) and frequency (Figures 3 and S7-S9) dependence below 35 K for **1·OH** and 25 K for **2·Cl** and **3·Br**, indicating a typical SMM behavior. Temperature-dependent out-of-phase (χ'') magnetic susceptibility signals exhibit peak at 27 K for **1·OH** and 19 K for **2·Cl** and **3·Br** (Figure S6). Upon cooling, χ'' signals increase rapidly at low temperature region, which could be attributed to quantum tunneling effects at zero dc field. Frequency-dependent magnetic susceptibility data under zero applied dc field show frequency-independent regime at 6.4, 24.1 and 62.9 Hz for **1·OH**, **2·Cl** and **3·Br**, respectively (Figure 3), confirming classical quantum tunneling. The quantum tunneling relaxation times τ_{QTM} were extracted as 24.9, 5.78 and 2.33 ms for **1·OH**, **2·Cl** and **3·Br**, respectively. When increasing the temperature, we find that the relaxation follows a thermally activated mechanism and the maxima of the out-of-phase χ'' peaks for all three complexes shift toward higher frequency. The τ *vs.* $1/T$ plots at high temperature were fitted with Arrhenius law [$\tau = \tau_0 \exp(U_{eff}/T)$], yielding anisotropy barriers U_{eff} of 168.2, 111.8 and 79.9 K for **1·OH**, **2·Cl** and **3·Br**, respectively. Accordingly, we fixed τ_{QTM} and U_{eff} to the above values to avoid the over parameterization and then fitted the entire temperature range using the following equation:[73-77]

$$\frac{1}{\tau_{obs}} = \frac{1}{\tau_{QTM}} + AH^2T + CT^n + \tau_0^{-1} \exp\left(\frac{-U_{eff}}{T}\right) \qquad (1)$$

where $1/\tau_{QTM}$, AH^2T, CT^n and $\tau_0 \cdot \exp(U_{eff}/T)$ represent quantum tunneling, direct, Raman and Orbach relaxation processes,[78, 79] respectively. Herein, the direct process is cancelled since the measurements were performed in the absence of a dc field. The best fits gave pre-exponential factors τ_0 of 6.59×10^{-7} (**1·OH**), 5.65×10^{-7} (**2·Cl**) and 4.13×10^{-6} s (**3·Br**). Other parameters obtained from the fitting are listed in Table S3.

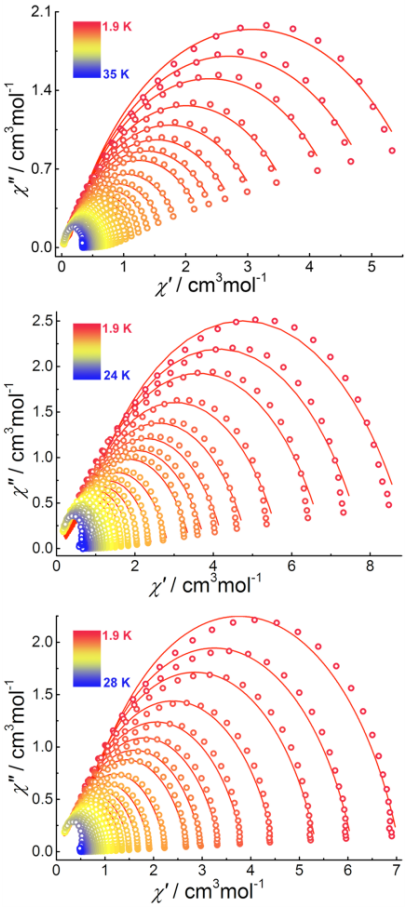

Figure 4. Cole-Cole plots for complexes **1·OH** (top), **2·Cl** (middle) and **3·Br** (bottom) at indicated temperatures under zero dc field. The solid lines indicate the best fits to the experiments with the generalized Debye model.

Cole–Cole plots of χ'' *vs.* χ' (Figure 4) reveal semicircular profiles, indicating a single relaxation process is operative for all complexes. The plots were fitted to a generalized Debye model with relatively small α parameters being in the range 0.04-0.26 (**1·OH**), 0.07-0.32 (**2·Cl**) and 0.08-0.24 (**3·Br**), indicating a very narrow distribution of relaxation times for each complex.[80-82]

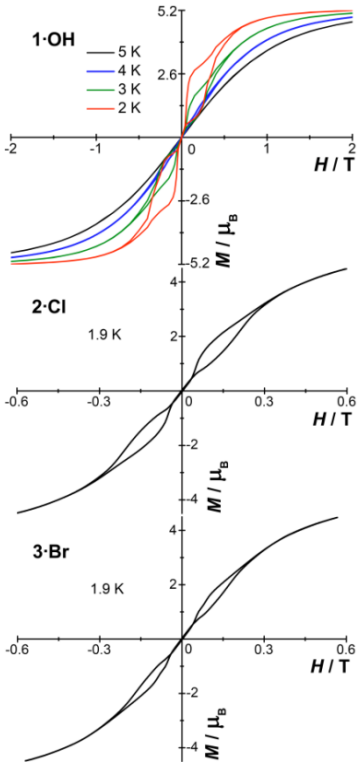

Figure 5. Magnetic hysteresis loops for **1·OH** (top), **2·Cl** (middle) and **3·Br** (bottom) with clear openings at $H \neq 0$.

We then probed the magnetic relaxation on polycrystalline samples of **1·OH**, **2·Cl** and **3·Br** via *M vs. H* hysteresis measurements, using a conventional SQUID magnetometer. As shown in Figure 5, all three complexes display clearly butterfly shaped magnetic hysteresis loops with openings up to 4 K for **1·OH** and 1.9 K for **2·Cl** and **3·Br** at $H \neq 0$, indicating the presence of magnetic blocking. The loss of the magnetization at zero field indicates the existence of quantum tunneling effect, which was apparent on the fast time scale (τ_{QTM}) of the dynamic ac experiment. The less opening ($H \neq 0$) of hysteresis loops at 1.9 K for **2·Cl** and **3·Br** suggest the much faster quantum tunneling than the one for **1·OH**. This is also coincident with the shorter quantum tunneling time τ_{QTM} for **2·Cl** and **3·Br** at zero field.

In order to reduce the dipole-dipole interactions between magnetic centers and slow down relaxation, magnetic dilution studies were performed on complexes **1·OH** and **2·Cl**. AC susceptibility measurements show great enhancement of the magnetic relaxation (Figures S10-S11), giving the effective energy barrier of 236.7 and 123.1 K for **1·OH** and **2·Cl**, respectively (Figure 6), which are much larger than the undiluted samples. The extracted τ_{QTM} are as long as 338.7 and 80.4 ms for **1·OH** and **2·Cl**, respectively, indicating the quantum tunneling at low temperature is also effectively suppressed. In addition, magnetic hysteresis measurements were also conducted on the diluted samples of **1·OH** and **2·Cl**. As expected, significant

improvements were observed (Figure 6). While, the hysteresis loops are still closed at zero filed, suggesting the intrinsic fast quantum tunneling, which is probably induced by the electronic structure and Hyperfine-Interaction.[49, 83]

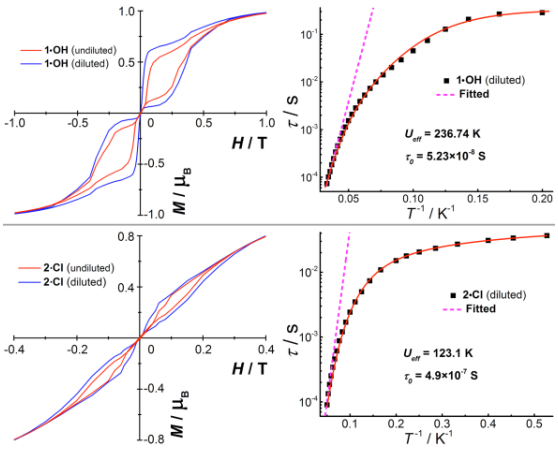

Figure 6. Magnetic hysteresis loops (left) and plots of τ *vs.* T^{-1} (right) for the diluted samples of **1·OH** (top) and **2·Cl** (bottom) at 1.9 K.

The coexistence of magnetic blocking and quantum tunneling in these complexes are possibly related with the structural features of each complex. As already inferred from the crystal structures, the variation of Dy-O_{sali} distances, $\angle O_{sali}$-Dy-O_{sali} angles and π···π stacking effects probably have critical impact on the electronic structure of the complex, thus should be responsible for the distinct magnetic anisotropy (Table 2). In complex **1·OH**, the relatively short Dy-O_{sali} distance and large $\angle O_{sali}$-Dy-O_{sali} angle profit for a strong axial crystal field, thus inducing a large energy barrier of magnetization reversion. While the π···π stacking effects between two Lz ligands might introduce large transversal components and short-cut fast relaxation process. For complexes **2·Cl** and **3·Br**, the Dy^{III} ions are in similar coordination environment, while the stronger π···π stacking effect would probably aggravate the quantum tunneling. Indeed, the quantum tunneling relaxation rates of **2·Cl** (2.33 ms) and **3·Br** (5.78 ms) are faster than that of **1·OH** (24.9 ms).

Table 2. Geometry parameters and energy barriers for the square antiprism dysprosium derivatives.

	O-Dy-O / °	Dy-O / Å	π···π / Å	ϕ / °	*CShM* (D_{4d})	τ_{QTM} / ms	U_{eff} / K
1·OH	149.018	2.203	3.826	58.646	1.327	24.9	168.2
2·Cl	142.855	2.247	3.596	46.946	0.643	5.78	111.8
3·Br	142.958	2.239	3.590	46.942	0.725	2.33	79.9

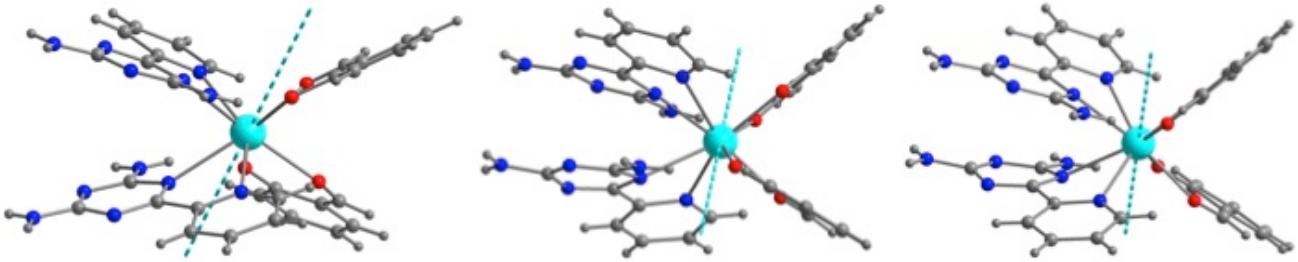

Figure 7. Orientation of the calculated main magnetic axes of the ground Kramers doublets on Dy^{III} centers in complexes **1·OH** (left), **2·Cl** (middle), and **3·Br** (right).

***Ab initio* Calculations.** Further insights into the electronic structure was performed by *ab initio* CASSCF/RASSI-SO calculations on the X-ray structures of **1·OH**, **2·Cl** and **3·Br** (see computational details). From the calculations, the energies of the eight Kramer doublets, the anisotropic tensors as well as the directions of the ground doublets were determined (see Tables S5-S7). As expected, in the three complexes, the multiplet ground state is $^6H_{15/2}$, with almost pure m_J = |±15/2> ground state. The isolated ground states and the minimum mixing of the m_J's in the first excited states are in line with the perfect Ising-type anisotropy of Dy^{III} center under the pseudo-D_{4d} coordinating crystal field. Moreover, the calculated $\chi_M T$ *vs.* T curves well reproduce the experimental ones (Figure 2). The calculated easy magnetic axes of ground state for the three compounds are represented in Figure 6. As expected, they lie in the most negatively charged direction *i.e.* almost parallel to O_{sali}-O_{sali} direction and correspond to a direction perpendicular to the pseudo C_2 axis. The deviation angle (β) between the magnetic axes of ground state and first excited state for **1·OH** (1.73°) is slightly smaller than those in **2·Cl** (2.27°) and **3·Br** (4.68°), suggesting a more axial ligand field and highlighting the importance of short Dy-O_{sali} distances and large $\angle O_{sali}$-

Dy-O_{sali} angles in **1·OH**. The computed magnetization blocking barriers in **1·OH**, **2·Cl** and **3·Br** are given in Figures S12-S14. They feature clearly thermally activated processes (Raman+Orbach) through the first and second excited states. The energy splitting of the $^6H_{15/2}$ ground multiplet is much larger in **1·OH** (229.32 cm^{-1} for first excited state) than in **2·Cl** (186.52 cm^{-1}, idem) and **3·Br** (166.61 cm^{-1}, idem), and the transition probability (through the barrier) are clearly smaller in **1·OH** than in the two other congeners. This could probably be ascribed to the less π···π stacking effect enhancing the energy splitting of the $^6H_{15/2}$ ground multiplet, which was demonstrated in our previous work.[57] Herein, the transition probability is directly related to the fast quantum tunneling relaxation. The much larger transversal components are coincident with the faster quantum tunneling relaxation in **2·Cl** and **3·Br** than in **1·OH** (*vide supra*).

CONCLUSION

In conclusion, three closely related dysprosium SMMs with mixed salicylaldehyde/pyridin-triazine ligands and discriminative counter-anion, **1·OH**, **2·Cl** and **3·Br**, are structurally and magnetically characterized. We find that the three complexes all possess similar square-antiprismatic geometry (D_{4d}) but display different dynamic magnetic properties. Each complex displayed a unique anisotropy barrier and quantum tunneling relaxation, with U_{eff} and τ_{QTM} in the ranges of 80-168 K and 2.3-25 ms, respectively. Structural and magnetic studies reveal that the magnetic anisotropy is dominated by the axial ligand field, highlighted by short Dy-O_{sali} distances and large ∠ O_{sali}-Dy-O_{sali} angles, while the quantum tunneling relaxation is probably dictated by the π···π stacking of the Lz ligands which results in an axial constriction of the coordinating plane. *Ab initio* calculations support the different magnetic behaviors in these complexes. It appears that strong axial ligand field and less stacking of the auxiliary ligands may provide the key for unlocking even higher excited state and prevent the magnetic quantum tunneling. Notably, the counter ion facilitates the modulation of the square-antiprismatic coordination geometry in this system, therefore, providing a possibility to promote anisotropy barriers and suppress the quantum tunneling effect. This work highlights the importance of axial ligand field and ligands stacking in obtaining larger energy barriers and controlling the quantum tunneling of Dy^{III} based SMMs with square-antiprismatic geometry.

ASSOCIATED CONTENT

Supporting Information.

Physical measurements; crystallography; computational details; structural, magnetic and calculated tables and figures. This material is available free of charge via the Internet at http://pubs.acs.org.

AUTHOR INFORMATION

Corresponding Authors

*Email: tang@ciac.ac.cn

*Email: boris.leguennic@univ-rennes1.fr

Notes

The authors declare no competing financial interest.

ACKNOWLEDGMENT

We thank the National Natural Science Foundation of China (Grants 21525103, 21371166, 21521092 and 21331003) for financial support. J.T. gratefully acknowledges support of the Royal Society-Newton Advanced Fellowship (NA160075).

REFERENCES

(1) Ishikawa, N.; Sugita, M.; Ishikawa, T.; Koshihara, S.-y.; Kaizu, Y. Lanthanide Double-Decker Complexes Functioning as Magnets at the Single-Molecular Level. *J. Am. Chem. Soc.* **2003** *125*, 8694-8695.

(2) Zhang, P.; Guo, Y.-N.; Tang, J. Recent advances in dysprosium-based single molecule magnets: Structural overview and synthetic strategies. *Coord. Chem. Rev.* **2013,** *257*, 1728-1763.

(3) Ungur, L.; Lin, S.-Y.; Tang, J.; Chibotaru, L. F. Single-molecule toroics in Ising-type lanthanide molecular clusters. *Chem. Soc. Rev.* **2014,** *43*, 6894-6905.

(4) Feltham, H. L. C.; Brooker, S. Review of purely 4f and mixed-metal nd-4f single-molecule magnets containing only one lanthanide ion. *Coord. Chem. Rev.* **2014,** *276*, 1-33.

(5) Lin, S.-Y.; Guo, Y.-N.; Xu, G.-F.; Tang, J. Research Progress on Pure Lanthanide Single-Molecule Magnets. *Chin. J. Appl. Chem.* **2010,** *27*, 1365-1371.

(6) Sorace, L.; Benelli, C.; Gatteschi, D. Lanthanides in molecular magnetism: old tools in a new field. *Chem. Soc. Rev.* **2011,** *40*, 3092-3104.

(7) Woodruff, D. N.; Winpenny, R. E. P.; Layfield, R. A. Lanthanide Single-Molecule Magnets. *Chem. Rev.* **2013,** *113*, 5110-5148.

(8) Sessoli, R.; Powell, A. K. Strategies towards single molecule magnets based on lanthanide ions. *Coord. Chem. Rev.* **2009,** *253*, 2328-2341.

(9) Gatteschi, D. Anisotropic dysprosium. *Nat. Chem.* **2011,** *3*, 830-830.

(10) Carlin, R. L. *Magnetochemistry*. Springer-Verlag: 1986.

(11) Gatteschi, D.; Sessoli, R.; Villain, J. *Molecular Nanomagnets*. Oxford University Press: 2006.

(12) Zhang, P.; Tang, J. *Lanthanide Single Molecule Magnets*. Springer-Verlag: 2015.

(13) Blagg, R. J.; Muryn, C. A.; McInnes, E. J.; Tuna, F.; Winpenny, R. E. Single pyramid magnets: Dy5 pyramids with slow magnetic relaxation to 40 K. *Angew. Chem. Int. Ed.* **2011,** *50*, 6530-6533.

(14) Blagg, R. J.; Ungur, L.; Tuna, F.; Speak, J.; Comar, P.; Collison, D.; Wernsdorfer, W.; McInnes, E. J. L.; Chibotaru, L. F.; Winpenny, R. E. P. Magnetic relaxation pathways in lanthanide single-molecule magnets. *Nat. Chem.* **2013,** *5*, 673-678.

(15) Pugh, T.; Chilton, N. F.; Layfield, R. Antimony-Ligated Dysprosium Single-Molecule Magnets as Catalysts for Stibine Dehydrocoupling. *Chem. Sci.* **2016**.

(16) Pugh, T.; Chilton, N. F.; Layfield, R. A. A Low-Symmetry Dysprosium Metallocene Single-Molecule Magnet with a High Anisotropy Barrier. *Angew. Chem. Int. Ed.* **2016,** *55*, 11082-11085.

(17) Xiong, J.; Ding, H.-Y.; Meng, Y.-S.; Gao, C.; Zhang, X.-J.; Meng, Z.-S.; Zhang, Y.-Q.; Shi, W.; Wang, B.-W.; Gao, S. Hydroxide-bridged five-coordinate Dy^{III} single-molecule magnet

exhibiting the record thermal relaxation barrier of magnetization among lanthanide-only dimers. *Chem. Sci.* **2017,** *8*, 1288-1294.

(18) Rinehart, J. D.; Fang, M.; Evans, W. J.; Long, J. R. A N_2^{3-} Radical-Bridged Terbium Complex Exhibiting Magnetic Hysteresis at 14 K. *J. Am. Chem. Soc.* **2011,** *133*, 14236-14239.

(19) Rinehart, J. D.; Fang, M.; Evans, W. J.; Long, J. R. Strong exchange and magnetic blocking in N_2^{3-}-radical-bridged lanthanide complexes. *Nat. Chem.* **2011,** *3*, 538-542.

(20) Kahn, O. *Molecular magnetism*. VCH: 1993.

(21) Coulon, C.; Miyasaka, H.; Clérac, R. Single-Chain Magnets:Theoretical Approach and Experimental Systems. In *Single-Molecule Magnets and Related Phenomena*, Winpenny, R., Ed. Springer Berlin Heidelberg: 2006; Vol. 122, pp 163-206.

(22) Ungur, L.; Chibotaru, L. F. Strategies toward High-Temperature Lanthanide-Based Single-Molecule Magnets. *Inorg. Chem.* **2016,** *55*, 10043-10056.

(23) Guo, Y.-N.; Ungur, L.; Granroth, G. E.; Powell, A. K.; Wu, C.; Nagler, S. E.; Tang, J.; Chibotaru, L. F.; Cui, D. An NCN-pincer ligand dysprosium single-ion magnet showing magnetic relaxation via the second excited state. *Scientific Reports* **2014,** *4*, 5471.

(24) Guo, Y.-N.; Xu, G.-F.; Wernsdorfer, W.; Ungur, L.; Guo, Y.; Tang, J.; Zhang, H.-J.; Chibotaru, L. F.; Powell, A. K. Strong Axiality and Ising Exchange Interaction Suppress Zero-Field Tunneling of Magnetization of an Asymmetric Dy_2 Single-Molecule Magnet. *J. Am. Chem. Soc.* **2011,** *133*, 11948-11951.

(25) Lin, S.-Y.; Wernsdorfer, W.; Ungur, L.; Powell, A. K.; Guo, Y.-N.; Tang, J.; Zhao, L.; Chibotaru, L. F.; Zhang, H.-J. Coupling Dy_3 Triangles to Maximize the Toroidal Moment. *Angew. Chem. Int. Ed.* **2012,** *51*, 12767-12771.

(26) Xue, S.; Guo, Y.-N.; Ungur, L.; Tang, J.; Chibotaru, L. F. Tuning the Magnetic Interactions and Relaxation Dynamics of Dy_2 Single-Molecule Magnets. *Chem. Eur. J.* **2015,** *21*, 14099-14106.

(27) Xue, S.; Ungur, L.; Guo, Y.-N.; Tang, J.; Chibotaru, L. F. Field-Induced Multiple Relaxation Mechanism of $Co^{III}_2Dy^{III}$ Compound with the Dysprosium Ion in a Low-Symmetrical Environment. *Inorg. Chem.* **2014,** 53, 12658-12663.

(28) Zhang, P.; Zhang, L.; Tang, J. Lanthanide single molecule magnets: Progress and perspective. *Dalton Trans.* **2015,** *44*, 3923-3929.

(29) Sessoli, R. Toward the Quantum Computer: Magnetic Molecules Back in the Race. *ACS Central Science* **2015,** *1*, 473-474.

(30) Gatteschi, D.; Sessoli, R. Quantum Tunneling of Magnetization and Related Phenomena in Molecular Materials. *Angew. Chem. Int. Ed.* **2003,** *42*, 268-297.

(31) Ishikawa, N.; Sugita, M.; Wernsdorfer, W. Quantum Tunneling of Magnetization in Lanthanide Single-Molecule Magnets: Bis(phthalocyaninato)terbium and Bis(phthalocyaninato)dysprosium Anions. *Angew. Chem. Int. Ed.* **2005,** *44*, 2931-2935.

(32) Leuenberger, M. N.; Loss, D. Quantum computing in molecular magnets. *Nature* **2001,** *410*, 789-793.

(33) Thiele, S.; Balestro, F.; Ballou, R.; Klyatskaya, S.; Ruben, M.; Wernsdorfer, W. Electrically driven nuclear spin resonance in single-molecule magnets. *Science* **2014,** *344*, 1135-1138.

(34) Ding, Y.-S.; Chilton, N. F.; Winpenny, R. E. P.; Zheng, Y.-Z. On Approaching the Limit of Molecular Magnetic Anisotropy: A Near-Perfect Pentagonal Bipyramidal Dysprosium(III) Single-Molecule Magnet. *Angew. Chem. Int. Ed.* **2016,** *55*, 16071-16074.

(35) Jiang, S.-D.; Wang, B.-W.; Sun, H.-L.; Wang, Z.-M.; Gao, S. An Organometallic Single-Ion Magnet. *J. Am. Chem. Soc.* **2011,** *133*, 4730-4733.

(36) Guo, F.-S.; Day, B. M.; Chen, Y.-C.; Tong, M.-L.; Mansikkamäki, A.; Layfield, R. A. A Dysprosium Metallocene Single-Molecule Magnet Functioning at the Axial Limit. *Angew. Chem. Int. Ed.*, Doi: 10.1002/anie.201705426.

(37) Chilton, N. F.; Collison, D.; McInnes, E. J. L.; Winpenny, R. E. P.; Soncini, A. An electrostatic model for the determination of magnetic anisotropy in dysprosium complexes. *Nat. Commun.* **2013,** *4*, 2551.

(38) Rinehart, J. D.; Long, J. R. Exploiting single-ion anisotropy in the design of f-element single-molecule magnets. *Chem. Sci.* **2011,** *2*, 2078-2085.

(39) Meng, Y.-S.; Jiang, S.-D.; Wang, B.-W.; Gao, S. Understanding the Magnetic Anisotropy toward Single-Ion Magnets. *Acc. Chem. Res.* **2016,** *49*, 2381-2389.

(40) Zhang, P.; Zhang, L.; Wang, C.; Xue, S.; Lin, S.-Y.; Tang, J. Equatorially Coordinated Lanthanide Single Ion Magnets. *J. Am. Chem. Soc.* **2014,** *136*, 4484-4487.

(41) Sun, W.; Yan, P.; Jiang, S.-D.; Wang, B.-W.; Zhang, Y.; Li, H.; Chen, P.; Wang, Z.-M.; Gao, S. High Symmetry or Low Symmetry, It Is a Question - High Performance Dy(III) Single-ion Magnets by Electrostatic Potential Design. *Chem. Sci.* **2015,** *7*, 684-691.

(42) Chen, Y.-C.; Liu, J.-L.; Ungur, L.; Liu, J.; Li, Q.-W.; Wang, L.-F.; Ni, Z.-P.; Chibotaru, L. F.; Chen, X.-M.; Tong, M.-L. Symmetry-Supported Magnetic Blocking at 20 K in Pentagonal Bipyramidal Dy(III) Single-Ion Magnets. *J. Am. Chem. Soc.* **2016,** *138*, 2829-2837.

(43) Liu, J.; Chen, Y.-C.; Liu, J.-L.; Vieru, V.; Ungur, L.; Jia, J.-H.; Chibotaru, L. F.; Lan, Y.; Wernsdorfer, W.; Gao, S.; Chen, X.-M.; Tong, M.-L. A Stable Pentagonal Bipyramidal Dy(III) Single-Ion Magnet with a Record Magnetization Reversal Barrier over 1000 K. *J. Am. Chem. Soc.* **2016,** *138*, 5441-5450.

(44) Gupta, S. K.; Rajeshkumar, T.; Rajaraman, G.; Murugavel, R. An Air-Stable Dy(III) Single-Ion Magnet with High Anisotropy Barrier and Blocking Temperature. *Chem. Sci.* **2016,** *7*, 5181-5191.

(45) Long, J.; Shestakov, B. G.; Liu, D.; Chibotaru, L.; Guari, Y.; Cherkasov, A.; Fukin, G. K.; Trifonov, A.; Larionova, J. An organolanthanide(III) single-molecule magnet with an axial crystal-field: influence of the Raman process over the slow relaxation. *Chem. Commun.* **2017**.

(46) Oyarzabal, I.; Ruiz, J.; Ruiz, E.; Aravena, D.; Seco, J. M.; Colacio, E. Increasing the effective energy barrier promoted by the change of a counteranion in a Zn-Dy-Zn SMM: slow relaxation via the second excited state. *Chem. Commun.* **2015,** *51*, 12353-12356.

(47) Ungur, L.; Chibotaru, L. F. Ab Initio Crystal Field for Lanthanides. *Chem. Eur. J.* **2017,** *23*, 3708-3718.

(48) Jiang, S.-D.; Wang, B.-W.; Su, G.; Wang, Z.-M.; Gao, S. A Mononuclear Dysprosium Complex Featuring Single-Molecule-Magnet Behavior. *Angew. Chem. Int. Ed.* **2010,** *49*, 7448-7451.

(49) Pointillart, F.; Bernot, K.; Golhen, S.; Le Guennic, B.; Guizouarn, T.; Ouahab, L.; Cador, O. Magnetic Memory in an Isotopically Enriched and Magnetically Isolated Mononuclear Dysprosium Complex. *Angew. Chem. Int. Ed.* **2015,** *54*, 1504-1507.

(50) Ou-Yang, J. K.; Saleh, N.; Fernandez Garcia, G.; Norel, L.; Pointillart, F.; Guizouarn, T.; Cador, O.; Totti, F.; Ouahab, L.; Crassous, J.; Le Guennic, B. Improved slow magnetic relaxation in optically pure helicene-based Dy^{III} single molecule magnets. *Chem. Commun.* **2016,** *52*, 14474-14477.

(51) Cosquer, G.; Pointillart, F.; Golhen, S.; Cador, O.; Ouahab, L. Slow Magnetic Relaxation in Condensed versus Dispersed Dysprosium(III) Mononuclear Complexes. *Chem. Eur. J.* **2013,** *19*, 7895-7903.

(52) Bi , Y.; Guo, Y.-N.; Zhao, L.; Guo, Y.; Lin, S.-Y.; Jiang, S.-D.; Tang, J.; Wang, B.-W.; Gao, S. Capping Ligand Perturbed Slow

Magnetic Relaxation in Dysprosium Single-Ion Magnets. *Chem. Eur. J.* **2011,** *17*, 12476-12481.

(53) Chen, G.-J.; Guo, Y.-N.; Tian, J.-L.; Tang, J.; Gu, W.; Liu, X.; Yan, S.-P.; Cheng, P.; Liao, D.-Z. Enhancing Anisotropy Barriers of Dysprosium(III) Single-Ion Magnets. *Chem. Eur. J.* **2012,** *18*, 2484-2487.

(54) Pointillart, F.; Jung, J.; Berraud-Pache, R.; Le Guennic, B.; Dorcet, V.; Golhen, S.; Cador, O.; Maury, O.; Guyot, Y.; Decurtins, S.; Liu, S.-X.; Ouahab, L. Luminescence and Single-Molecule Magnet Behavior in Lanthanide Complexes Involving a Tetrathiafulvalene-Fused Dipyridophenazine Ligand. *Inorg. Chem.* **2015,** *54*, 5384-5397.

(55) Zhang, S.; Ke, H.; Sun, L.; Li, X.; Shi, Q.; Xie, G.; Wei, Q.; Yang, D.; Wang, W.; Chen, S. Magnetization Dynamics Changes of Dysprosium(III) Single-Ion Magnets Associated with Guest Molecules. *Inorg. Chem.* **2016,** 55, 3865-3871.

(56) da Cunha, T. T.; Jung, J.; Boulon, M.-E.; Campo, G.; Pointillart, F.; Pereira, C. L. M.; Le Guennic, B.; Cador, O.; Bernot, K.; Pineider, F.; Golhen, S.; Ouahab, L. Magnetic Poles Determinations and Robustness of Memory Effect upon Solubilization in a DyIII-Based Single Ion Magnet. *J. Am. Chem. Soc.* **2013,** *135*, 16332-16335.

(57) Wu, J.; Jung, J.; Zhang, P.; Zhang, H.; Tang, J.; Le Guennic, B. Cis-Trans Isomerism Modulates the Magnetic Relaxation of Dysprosium Single-Molecule Magnets. *Chem. Sci.* **2016,** *7*, 3632-3639.

(58) Case, F. H.; Koft, E. The Synthesis of Certain Substituted 1,3,5-Triazines Containing the Ferroin Group. *J. Am. Chem. Soc.* **1959,** *81*, 905-906.

(59) Sheldrick, G. M. *SHELXS-97 Program for Crystal Structure Solution*. University of Göttingen: Germany: 1997.

(60) Sheldrick, G. M. A short history of SHELX. *Acta Crystallogr., Sect. A* **2008,** *64*, 112-122.

(61) Boudreaux, E. A.; Mulay, L. N. *Theory and Applications of Molecular Paramagnetism*. John Wiley & Sons,: New York: 1976.

(62) Aquilante, F.; De Vico, L.; Ferré, N.; Ghigo, G.; Malmqvist, P.-å.; Neogrády, P.; Pedersen, T. B.; Pitoňák, M.; Reiher, M.; Roos, B. O.; Serrano-Andrés, L.; Urban, M.; Veryazov, V.; Lindh, R. MOLCAS 7: The Next Generation. *J. Comput. Chem.* **2010,** *31*, 224-247.

(63) Roos, B. O.; Taylor, P. R.; Siegbahn, P. E. M. A complete active space SCF method (CASSCF) using a density matrix formulated super-CI approach. *Chem. Phys.* **1980,** *48*, 157-173.

(64) Malmqvist, P.-Å.; Roos, B. O. The CASSCF state interaction method. *Chem. Phys. Lett.* **1989,** *155*, 189-194.

(65) Malmqvist, P. Å.; Roos, B. O.; Schimmelpfennig, B. The restricted active space (RAS) state interaction approach with spin–orbit coupling. *Chem. Phys. Lett.* **2002,** *357*, 230-240.

(66) Chibotaru, L. F.; Ungur, L. Ab initio calculation of anisotropic magnetic properties of complexes. I. Unique definition of pseudospin Hamiltonians and their derivation. *J. Chem. Phys.* **2012,** *137*, 064112.

(67) Chibotaru, L. F.; Ungur, L.; Soncini, A. The Origin of Nonmagnetic Kramers Doublets in the Ground State of Dysprosium Triangles: Evidence for a Toroidal Magnetic Moment. *Angew. Chem. Int. Ed.* **2008,** *47*, 4126-4129.

(68) Aquilante, F.; Malmqvist, P.-Å.; Pedersen, T. B.; Ghosh, A.; Roos, B. O. Cholesky Decomposition-Based Multiconfiguration Second-Order Perturbation Theory (CD-CASPT2): Application to the Spin-State Energetics of Co^{III}(diiminato)(NPh). *J. Chem. Theory Comput.* **2008,** *4*, 694-702.

(69) Roos, B. O.; Lindh, R.; Malmqvist, P.-Å.; Veryazov, V.; Widmark, P.-O. New Relativistic ANO Basis Sets for Transition Metal Atoms. *The Journal of Physical Chemistry A* **2005,** *109*, 6575-6579.

(70) Roos, B. O.; Lindh, R.; Malmqvist, P.-Å.; Veryazov, V.; Widmark, P.-O. Main Group Atoms and Dimers Studied with a New Relativistic ANO Basis Set. *The Journal of Physical Chemistry A* **2004,** *108*, 2851-2858.

(71) Roos, B. O.; Lindh, R.; Malmqvist, P.-Å.; Veryazov, V.; Widmark, P.-O.; Borin, A. C. New Relativistic Atomic Natural Orbital Basis Sets for Lanthanide Atoms with Applications to the Ce Diatom and LuF_3. *The Journal of Physical Chemistry A* **2008,** *112*, 11431-11435.

(72) Casanova, D.; Alemany, P.; Bofill, J. M.; Alvarez, S. Shape and Symmetry of Heptacoordinate Transition-Metal Complexes: Structural Trends. *Chem. Eur. J.* **2003,** *9*, 1281-1295.

(73) Lucaccini, E.; Sorace, L.; Perfetti, M.; Costes, J.-P.; Sessoli, R. Beyond the anisotropy barrier: slow relaxation of the magnetization in both easy-axis and easy-plane Ln(trensal) complexes. *Chem. Commun.* **2014,** 50, 1648-1651.

(74) Zadrozny, J. M.; Atanasov, M.; Bryan, A. M.; Lin, C.-Y.; Rekken, B. D.; Power, P. P.; Neese, F.; Long, J. R. Slow magnetization dynamics in a series of twocoordinate iron(II) complexes. *Chem. Sci.* **2013,** *4*, 125–138

(75) Li, X.-L.; Li, H.; Chen, D.-M.; Wang, C.; Wu, J.; Tang, J.; Shi, W.; Cheng, P. Planar Dy_3 + Dy_3 clusters: design, structure and axial ligand perturbed magnetic dynamics. *Dalton Trans.* **2015,** *44*, 20316-20320.

(76) Wu, J.; Zhao, L.; Guo, M.; Tang, J. Constructing supramolecular grids: from 4f square to 3d-4f grid. *Chem. Commun.* **2015,** *51*, 17317-17320.

(77) Wu, J.; Zhao, L.; Zhang, L.; Li, X.-L.; Guo, M.; Tang, J. Metallosupramolecular Coordination Complexes: The Design of Heterometallic 3d–4f Gridlike Structures. *Inorg. Chem.* **2016,** 55, 5514-5519.

(78) Orbach, R. Spin-Lattice Relaxation in Rare-Earth Salts: Field Dependence of the Two-Phonon Process. *Proc. R. Soc. Lond. A* **1961,** *264*, 485-495.

(79) Orbach, R. Spin-Lattice Relaxation in Rare-Earth Salts. *Proc. R. Soc. Lond. A* **1961,** *264*, 458-484.

(80) Li, X.-L.; Min, F.-Y.; Wang, C.; Lin, S.-Y.; Liu, Z.; Tang, J. Utilizing 3d–4f Magnetic Interaction to Slow the Magnetic Relaxation of Heterometallic Complexes. *Inorg. Chem.* **2015,** *54*, 4337-4344.

(81) Li, X.-L.; Wu, J.; Tang, J.; Le Guennic, B.; Shi, W.; Cheng, P. A planar triangular Dy_3 + Dy_3 single-molecule magnet with a toroidal magnetic moment. *Chem. Commun.* **2016,** *52*, 9570-9573.

(82) Wu, J.; Zhao, L.; Zhang, P.; Zhang, L.; Guo, M.; Tang, J. Linear 3d-4f Compounds: Synthesis, Structure, and Determination of the d-f Magnetic Interaction. *Dalton Trans.* **2015,** *44*, 11935-11942.

(83) Chen, Y.-C.; Liu, J.-L.; Wernsdorfer, W.; Liu, D.; Chibotaru, L. F.; Chen, X.-M.; Tong, M.-L. Hyperfine-Interaction-Driven Suppression of Quantum Tunneling at Zero Field in a Holmium(III) Single-Ion Magnet. *Angew. Chem. Int. Ed.* **2017,** *56*, 4996-5000.

SYNOPSIS TOC

Axial ligand field with short Dy-O_{sali} distance and less π-π stacking found in closely related dysprosium compounds with discriminative counter-anion where the metal in square-antiprismatic geometry suppress quantum tunneling and enhance the magnetic relaxation.